Thermal effects in hot and dilute homogeneous asymmetric nuclear matter

Vishal Parmar* and Manoj K. Sharma
School of Physics and Materials Science, Thapar Institute of Engineering and Technology, Patiala-147004, India

S. K. Patra
Institute of Physics, Bhubaneswar 751005, India
and Homi Bhaba National Institute, Training School Complex, Anushakti Nagar, Mumbai 400 085, India

(Received 24 January 2021; accepted 6 May 2021; published 26 May 2021)

We present an analysis of hot and dilute isospin-asymmetric nuclear matter employing the temperature-dependent effective-relativistic mean-field theory (E-RMF). We consider nuclear matter to be homogeneous and study the equation of state (EoS) for densities, temperature, and asymmetry which are relevant for astrophysical simulations such as supernovae explosion and neutron-star crust. The two recently developed E-RMF parameter sets IOPB-I and G3 are used here to study various physical observables at finite temperatures. These sets are known to reproduce the nuclear matter properties, in agreement with various experimental and observational constraints. The effect of temperature is investigated in reference to the density-dependent free symmetry energy and its higher-order derivatives using the well-known parabolic approximation. The larger value of λ_ω cross coupling in G3 in addition to the δ meson coupling in G3 smoothen the free symmetry energy. Thermal effects on various state variables are examined at fixed temperature and isospin asymmetry by separating their $T = 0$ and the finite-T expressions. The thermal effects are governed by effective mass where larger effective mass corresponds to larger thermal contribution. The effect of temperature on isothermal and isentropic incompressibility is discussed, which is in harmony with various microscopic calculations. The liquid-gas phase-transition properties are examined in asymmetric matter in the context of different slope parameter and comparable symmetry energy in the IOPB-I and G3 set. The spinodal instability, binodal curve, and critical properties are found to be influenced by the slope parameter $L_{\rm sym}$. Finally, we consider a more realistic system (with the inclusion of electrons) and analyze the effect on instability and adiabatic index of isospin asymmetric nuclear matter.

DOI: 10.1103/PhysRevC.103.055817

I. INTRODUCTION

Core-collapse supernovae represent the end product of the stellar evolution of massive stars ($M > 8M_\odot$), leading to a very luminous explosion and the formation of a neutron star [1,2]. The exact mechanism of the collapse explosion is still not well understood even after several decades of thorough investigations. In recent years, such explosions have been studied using several *ab initio* core-collapse simulations where the hydrodynamics equations are solved numerically [3,4]. These simulations estimate that the explosion energy of $\approx 10^{51}$ erg is attained within the timescale of $\geqslant 1$ s [5]. The temperature of the matter rises to 20 MeV and the density of the bounce can vary up to two times the nuclear saturation density. The short timescale of collapse does not allow the matter to reach β equilibrium and calculations are usually done at a fixed asymmetry $\alpha = \frac{\rho_n - \rho_p}{\rho_n + \rho_p} \approx 0.4$ [6,7].

The determination of EoS for isospin-asymmetric nuclear matter (ANM) is relevant in various areas of nuclear physics ranging from finite nuclei to infinite matter. Not only the understanding of its ground state is important, but its behavior at finite temperature is equally significant. The finite-temperature behavior of ANM is relevant in context to astrophysical events such as neutron-star mergers, γ-ray bursts, proto-neutron stars, early universe, etc. [8]. Furthermore, the composition of matter inside the neutron star impacts its transportation and cooling process which are governed by the so-called direct URCA process [9]. With the recent detection of gravitational waves (GW170817) which were accompanied by a γ-ray-burst and electromagnetic afterglow from the merger of a neutron-star binary opened a new era of astrophysics [10,11]. In view of the above, a systematic understanding of asymmetric nuclear matter at finite temperature is highly desirable.

The nuclear matter which is predominantly governed by a residual short-range strong force and a long-range electromagnetic interaction shows various structures which in turn depend upon the parameters such as density, asymmetry, and temperature. At low temperature or entropy, the matter is in the nonhomogeneous form below the subnuclear density ($\rho < 0.1$ fm^{-3}). The nuclear matter is a mixture of heavy nuclei and light clusters in a background of nucleon gas [12]. As the density increases, the nuclei become deformed, constituting a frustrated system usually known as pasta structures because of the competition between nuclear and

*physics.vishal01@gmail.com

electromagnetic forces [13]. Above saturation density, the matter converts to a homogeneous mixture of nucleons which may contain exotic species such as kaon and pion condensate, hyperons, and quark phases. Leptons (electrons in low density and electrons with muons at high density) are present in all these structures for charge neutrality. At large-enough temperatures, the nonhomogeneous nuclear matter at low density again transforms to the homogeneous phase. In this work, however, we assume the nuclear matter to be an ideal homogeneous mixture of nucleons. Such an investigation of an ideal ANM system is significant to understand the underlying qualitative behavior. We employ the finite-temperature extension of the effective-relativistic mean-field theory (E-RMF) to study the asymmetric nuclear matter at finite temperature. The recently developed E-RMF parameters, namely, IOPB-I [14] and G3 [15], are used here to understand various aspects of nuclear matter at finite temperature. These sets have comparable saturation properties at zero temperature but differ in the number of adjustable parameters, i.e., various self and cross couplings of σ, ω, ρ, and δ mesons. This provides us with an opportunity to study the effect of these couplings on the finite-temperature properties of asymmetric nuclear matter.

The central motivation of this study is to perform a detailed analysis of the EoS for dilute and hot homogeneous asymmetric nuclear matter within the E-RMF formalism. We aim to understand the nuclear matter properties like symmetry energy $F_{\rm sym}$, slope parameter $L_{\rm sym}$, skewness parameter $Q_{\rm sym}$, and curvature parameter $K_{\rm sym}$ as a function of temperature. These are significant properties of asymmetric nuclear matter and are often used to constraint the EoS around saturation density. Several finite-temperature effects such as thermal effects on various state variables and on isothermal and isentropic incompressibility are addressed. The results presented in this study (below subnuclear density) serve only to differentiate between the realistic nonhomogeneous phase in a supernova and ideal homogeneous phase. This is analogous to the van der Waals equation of state and ideal-gas equation in atomic physics. The phase-transition property in asymmetric matter in comparison with symmetric matter is discussed in the context of incompressibility K and slope parameter $L_{\rm sym}$. With this study, we aim to verify the trends available in various studies [6,16–18], where the effect is discussed of symmetry energy and its derivative on the instability of ANM. Establishing these trends is of primary importance because they serve as the bridge between various nuclear matter properties which are not measured directly in experiments. In symmetric nuclear matter (SNM), the trends are seen among the properties at critical temperature [19]. The properties at ground state do not necessarily dictate the critical properties of phase transition. However, for asymmetric matter, the symmetry energy and its slope parameter decides the energetics and therefore impacts the instabilities occurring in the system. In a realistic case like a supernovae it will affect the transportation and cooling process whereas, in neutron-star crust, the core-crust boundary becomes the variable of the slope parameter $L_{\rm sym}$.

The paper is organized as follows: In Sec. II, we give a brief formalism of the E-RMF model at finite temperature. The thermal effects on various thermodynamic functions and stability conditions are mentioned in this section. In Sec. III, we summarize our results where we discuss the model properties in Sec. III A and properties at finite temperature in Sec. III B. We discuss the liquid-gas phase transition in ANM in Sec. III C. In Sec. III D, we discuss the influence of electrons on the EoS. Finally, we summarize our results in Sec. IV.

II. FORMALISM

The Lagrangian and the corresponding energy-density functional of the effective field theory (EFT) motivated E-RMF is documented in the literature [14,15,19,20]. The advantage of the E-RMF formalism is that one can ignore the basic difficulties of the formalism, like renormalization and divergence of the system. It takes care of several natural phenomena in *ab initio* manner which otherwise are absent or are included in an *ad hoc* manner in nonrelativistic formalisms. In the effective nuclear field theory, the Lagrangian contains an infinite number of terms. The Lagrangian is expanded in the power of meson fields as a truncation scheme because the fields have a lower mass compared with nucleon masses. The contribution of each term in the E-RMF Lagrangian can be calculated by counting the power of expansion. Couplings present at a particular order cannot be dropped arbitrarily without a proper symmetry argument. The ambiguity in the expansion is checked by the inclusion of naturalness constraints and naive dimensional analysis (NDA). For calibration, the coupling constants and mass of isoscalar-scalar σ meson are fit to reproduce the experimental values of the saturation density and the ground-state properties of some known nuclei. This method mocks the result of two-loop contribution in mean-field theory [21]. The basic nucleon-meson E-RMF which involve couplings of σ, ω, ρ, and δ mesons and the photon with Dirac nucleon up to the fourth order is given as [19]

$$
\begin{aligned}
\mathcal{E}(r) = {} & \psi^{\dagger}(r)\left\{ i\alpha\cdot\nabla + \beta[M - \Phi(r) - \tau_3 D(r)] + W(r) + \frac{1}{2}\tau_3 R(r) + \frac{1+\tau_3}{2}A(r) - \frac{i\beta\alpha}{2M}\left(f_\omega \nabla W(r) + \frac{1}{2}f_\rho \tau_3 \nabla R(r)\right)\right\}\psi(r) \\
& + \left(\frac{1}{2} + \frac{k_3\Phi(r)}{3!M} + \frac{k_4}{4!}\frac{\Phi^2(r)}{M^2}\right)\frac{m_s^2}{g_s^2}\Phi(r)^2 - \frac{\zeta_0}{4!}\frac{1}{g_\omega^2}W(r)^4 + \frac{1}{2g_s^2}\left(1 + \alpha_1\frac{\Phi(r)}{M}\right)[\nabla\Phi(r)]^2 \\
& - \frac{1}{2g_\omega^2}\left(1 + \alpha_2\frac{\Phi(r)}{M}\right)[\nabla W(r)]^2 - \frac{1}{2}\left(1 + \eta_1\frac{\Phi(r)}{M} + \frac{\eta_2}{2}\frac{\Phi^2(r)}{M^2}\right)\frac{m_\omega^2}{g_\omega^2}W^2(r) - \frac{1}{2e^2}(\nabla A^2(r))^2 \\
& - \frac{1}{2g_\rho^2}[\nabla R(r)]^2 - \frac{1}{2}\left(1 + \eta_\rho\frac{\Phi(r)}{M}\right)\frac{m_\rho^2}{g_\rho^2}R^2(r) - \Lambda_\omega(R^2(r)W^2(r)) + \frac{1}{2g_\delta^2}[\nabla D(r)]^2 + \frac{1}{2}\frac{m_\delta^2}{g_\delta^2}[D(r)]^2. \qquad (1)
\end{aligned}
$$

Here $\Phi(r)$, $W(r)$, $R(r)$, $D(r)$, and $A(r)$ are the fields corresponding to σ, ω, ρ, and δ mesons and photons, respectively. The g_s, g_ω, g_ρ, g_δ, and $\frac{e^2}{4\pi}$ are the corresponding coupling constants and m_s, m_ω, m_ρ, and m_δ are the corresponding masses. The zeroth component $T_{00} = H$ and the third component T_{ii} of the energy-momentum tensor

$$T_{\mu\nu} = \partial^\nu \phi(x) \frac{\partial \mathcal{E}}{\partial \partial_\mu \phi(x)} - \eta^{\nu\mu}\mathcal{E}, \tag{2}$$

yields the energy and pressure density, respectively, as

$$E = \sum_{p,n} \frac{\gamma}{(2\pi)^3} \int d^3k E^*_{p,n}(k)[n_k(T) + \bar{n}_k(T)] + \rho W + \left(\frac{1}{2} + \frac{k_3\Phi}{3!M} + \frac{k_4}{4!}\frac{\Phi^2}{M^2}\right)\frac{m_s^2}{g_s^2}\Phi^2 - \frac{1}{2}\left(1 + \eta_1\frac{\Phi}{M} + \frac{\eta_2}{2}\frac{\Phi^2}{M^2}\right)\frac{m_\omega^2}{g_\omega^2}W^2$$
$$- \frac{\zeta_0}{4!}\frac{1}{g_\omega^2}W^4 + \frac{1}{2}\rho_3 R - \frac{1}{2}\left(1 + \eta_\rho\frac{\Phi}{M}\right)\frac{m_\rho^2}{g_\rho^2}R^2 - \Lambda_\omega(R^2W^2) + \frac{1}{2}\frac{m_\delta^2}{g_\delta^2}(D)^2, \tag{3}$$

$$P = \sum_{p,n} \frac{\gamma}{3(2\pi)^3} \int d^3k \frac{k^2}{E^*_{p,n}(k)}[n_k(T) + \bar{n}_k(T)] - \left(\frac{1}{2} + \frac{k_3\Phi}{3!M} + \frac{k_4}{4!}\frac{\Phi^2}{M^2}\right)\frac{m_s^2}{g_s^2}\Phi^2 + \frac{1}{2}\left(1 + \eta_1\frac{\Phi}{M} + \frac{\eta_2}{2}\frac{\Phi^2}{M^2}\right)\frac{m_\omega^2}{g_\omega^2}W^2$$
$$+ \frac{\zeta_0}{4!}\frac{1}{g_\omega^2}W^4 + \frac{1}{2}\left(1 + \eta_\rho\frac{\Phi}{M}\right)\frac{m_\rho^2}{g_\rho^2}R^2 + \Lambda_\omega(R^2W^2) - \frac{1}{2}\frac{m_\delta^2}{g_\delta^2}(D)^2. \tag{4}$$

In the above equations, $n_k(T)$ and $\bar{n}_k(T)$ are the baryon and antibaryon occupation numbers, respectively, which are defined by the Fermi distribution function at finite temperature T as

$$n_k(T) = \frac{1}{1 + \exp\left(\frac{E^*(k) - \nu}{T}\right)}, \tag{5a}$$

$$\bar{n}_k(T) = \frac{1}{1 + \exp\left(\frac{E^*(k) + \nu}{T}\right)}, \tag{5b}$$

with E^* as $(k^2 + M^{*2})^{1/2}$. Here the effective mass is written as [22]

$$M_p^* = M - \Phi(r) - D(r), \tag{6a}$$

$$M_n^* = M - \Phi(r) + D(r). \tag{6b}$$

The effective chemical potential ν for protons and neutrons is defined as

$$\nu_p = \mu - W(r) + \tfrac{1}{2}R(r), \tag{7a}$$

$$\nu_n = \mu - W(r) - \tfrac{1}{2}R(r). \tag{7b}$$

The entropy density ($S = s/\rho_b$) is given as

$$s_i = -2\sum_i \int \frac{d^3k}{(2\pi)^3}[n_k \ln n_k + (1 - n_k)\ln(1 - n_k) + (n_k \leftrightarrow \bar{n}_k)], \tag{8}$$

and the free energy is defined as

$$F = E - TS. \tag{9}$$

The free-energy density can be written in the parabolic form of the asymmetry parameter ($\alpha = \frac{\rho_n - \rho_p}{\rho_n + \rho_p}$) as [23,24]

$$F(\rho, \alpha, T) = F(\rho, \alpha = 0, T) + F_{\rm sym}(\rho, T)\alpha^2, \tag{10}$$

where $F_{\rm sym}(\rho, T)\alpha^2$ is the free symmetry energy content per nucleon of the system and $F(\rho, \alpha = 0, T)$ is the free energy per nucleon of symmetric ($\alpha = 0$) nuclear matter. The free symmetric energy using the empirical parabolic approximation then can be written as

$$F_{\rm sym}(\rho, T) = \frac{F(\rho, T, \alpha = 1)}{\rho} - \frac{F(\rho, T, \alpha = 0)}{\rho}. \tag{11}$$

The free symmetric energy then can be expanded as a Taylor series around the saturation density ρ_0 as

$$F_{\rm sym}(\rho, T) = F_{\rm sym}(\rho_0, T) + L_{\rm sym}\S + \frac{K_{\rm sym}}{2!}\S^2 + \frac{Q_{\rm sym}}{3!}\S^3 + O(\S^4), \tag{12}$$

where $\S = \frac{\rho - \rho_0}{3\rho_0}$ and $L_{\rm sym}$, $K_{\rm sym}$, and $Q_{\rm sym}$ are the slope parameter, curvature parameter, and skewness parameter, which are written as

$$L_{\rm sym} = 3\rho\frac{\partial F_{\rm sym}(\rho, T)}{\partial\rho},$$

$$K_{\rm sym} = 9\rho^2\frac{\partial^2 F_{\rm sym}(\rho, T)}{\partial\rho^2},$$

$$Q_{\rm sym} = 27\rho^3\frac{\partial^3 F_{\rm sym}(\rho, T)}{\partial\rho^3}. \tag{13}$$

To infer the effects of finite temperature we focus on the thermal part of the various state variables; that is, the difference between the $T = 0$ and the finite-T expressions for a given thermodynamic function $\mathcal{X}$ [25,26],

$$\mathcal{X} = \mathcal{X}(\rho, \alpha, T) - \mathcal{X}(\rho, \alpha, 0). \tag{14}$$

The thermal energy, thermal pressure, thermal free-energy density, and thermal index are then written as

$$E_{th} = E(\alpha, T) - E(\alpha, 0),$$
$$P_{th} = P(\alpha, T) - P(\alpha, 0),$$
$$F_{th} = F(\alpha, T) - E(\alpha, 0),$$
$$\lambda_{th} = 1 + \frac{E_{th}}{P_{th}}. \tag{15}$$

Thermal contributions to the free symmetry energy are given by

$$F_{\rm sym,th} = F_{\rm sym}(\alpha, T) - E_{\rm sym}(\alpha, 0). \tag{16}$$

In asymmetric nuclear matter system, there are two conserved charges, baryon number B($\rho_b = \rho_p + \rho_n$) and isospin number ($I_3 = I_p + I_n$). Therefore, one needs to treat it as a binary system. The system will be stable against separation into two phases if the free energy of a single phase is lower than the free energy in all multiphase configurations. This is formulated as

$$\mathcal{F}(T, \rho_i) < (1-\lambda)\mathcal{F}(T, \rho_i{}') + \lambda\mathcal{F}(T, \rho_i{}''), \tag{17}$$

with

$$\rho_i = (1-\lambda)\rho_i{}' + \lambda\rho_i{}'', \tag{18}$$

where the two phases are denoted by prime and double prime and λ is the volume fraction. In formal terms, stability implies that the free-energy density is a convex function of the density. Convexity implies that the stability against separation into two phases also guarantees stability against separation into an arbitrary number of phases. In other terms, it is necessarily true that the symmetric matrix [27]

$$\mathcal{F}_{ij} = \left(\frac{\partial^2 \mathcal{F}}{\partial\rho_i \partial\rho_j}\right)_T \tag{19}$$

is positive. This results in mechanical and diffusive stability conditions as

$$\left.\frac{\partial P}{\partial \rho_b}\right|_{T,\alpha} > 0 \text{ and } \left.\frac{\partial \mu_p}{\partial \alpha}\right|_{T,P} < 0. \tag{20}$$

If one of the stability conditions is violated, a system with two phases is energetically favorable. The phase coexistence is governed by the Gibbs conditions

$$\begin{aligned} \mu_q'(T, \rho_b') &= \mu_q''(T, \rho_b'') \ (q = n, p), \\ P'(T, \rho_b') &= P''(T, \rho_b''). \end{aligned} \tag{21}$$

At the critical points, the pressure, density and temperature are written as P_c, ρ_c, and T_c. For asymmetric nuclear matter, they are calculated by finding an inflation point at chemical-potential isobars as

$$\left.\frac{\partial \mu_q}{\partial \alpha}\right|_{T=T_c} = \left.\frac{\partial^2 \mu_q}{\partial \alpha^2}\right|_{T=T_c} = 0. \tag{22}$$

Furthermore, one can define isothermal incompressibility of nuclear matter at finite temperature T and asymmetry α as

$$K^T(\alpha, T) = 9\left(\rho_b^2 \frac{\partial^2 F}{\partial \rho_b^2}\right)\Big|_{\rho_b^T(\alpha,T)}. \tag{23}$$

Here, ρ_b^T is the density where free energy has its minimum. The isentropic incompressibility at entropy S and asymmetry α which is an important quantity in supernova collapse is written as [28]

$$K^S(\alpha, S) = 9\left(\rho_b^2 \frac{\partial^2 E}{\partial \rho_b^2}\right)\Big|_{\rho_b^T(\alpha,S)}. \tag{24}$$

TABLE I. Bulk-matter properties of nuclear matter for the IOPB-I and G3 parameter and their corresponding empirical values.

	IOPB-I	G3	Empirical value
ρ_0 (fm^{-3})	0.149	0.148	0.148–0.185 [30]
E_0 (MeV)	−16.10	−16.02	−15.0– − 17.0 [30]
M^*/M	0.593	0.699	0.55–0.6 [31]
J (MeV)	33.30	31.84	30.0–33.7 [32]
L (MeV)	63.58	49.31	35.0–70.0 [32]
$K_{\rm sym}$ (MeV)	−37.09	−106.07	−174.0– − 31.0 [33]
$Q_{\rm sym}$ (MeV)	862.70	915.47	−494.0– − 10.0 [34]
K (MeV)	222.65	243.96	220.0–260.0 [35]

III. RESULTS AND DISCUSSIONS

A. Model properties

In this work, we consider two recent E-RMF parameters, namely, IOPB-I [14] and G3 [15]. The IOPB-I set contains the quartic-order cross-coupling $R(r)^2W(r)^2$ ($\lambda_\omega \neq 0$) and self-coupling of isoscalar-vector $W(r)^2$ (ζ_0). This set produces the infinite nuclear matter properties at saturation and supersaturation density, which is consistent with the empirical data. The maximum mass is found to be $2.15M_\odot$ which satisfies the current GW170817 observational constraint. The G3 set, on the other hand, is the most comprehensive parameter that contains all the nucleons and tensor coupling terms in addition to several self- and cross-coupling components. It is known to estimate neutron-skin thickness over a wide range, in harmony with the experimental data. It estimates the maximum neutron-star mass $2.03M_\odot$ with a canonical mass radius of 12.69 km, which is a desirable feature in the context of observational analysis and finite-nuclei experiments. The main feature of the set G3 is that it includes the couplings of nucleons to the δ and ρ mesons and cross-couplings of $\sigma\omega$ and $\sigma\rho$ mesons. The G3 set has positive scalar self couplings k_3 and k_4 and ζ_0 nearly equal to 1. The G3 set and IOPB-I set also differ in the value of λ_ω. IOPB-I has relatively small λ_ω as compared with G3. In Table I, we present the bulk matter properties of nuclear matter for the G3 and IOPB-I sets and the corresponding empirical values. It is clear that these sets satisfy the well-accepted set of laboratorial, theoretical, and observational constraints.

In Fig. 1 we compare the neutron matter binding energy and pressure with the microscopic calculations based on chiral effective-field theory (EFT) with realistic two- and three-nucleon interactions [29]. The inner graph represents the difference between the neutron matter energy and pressure and the average energy and pressure normalized to the uncertainty of the microscopic calculations ($\sigma = \delta P$). The uncertainties are represented by the orange band, and they indicate that the points that lie inside this band are within the 1σ error limits. The G3 set satisfies nicely the microscopic constraints whereas IOPB-I also falls within the 1σ error limit below saturation density. Both of these parameters also satisfy the constraint from collective flow data in heavy-ion collisions and kaon experiments along with the GW170817 gravitational wave constraints [14]. These features along with the agreement of bulk-matter properties with empirical data

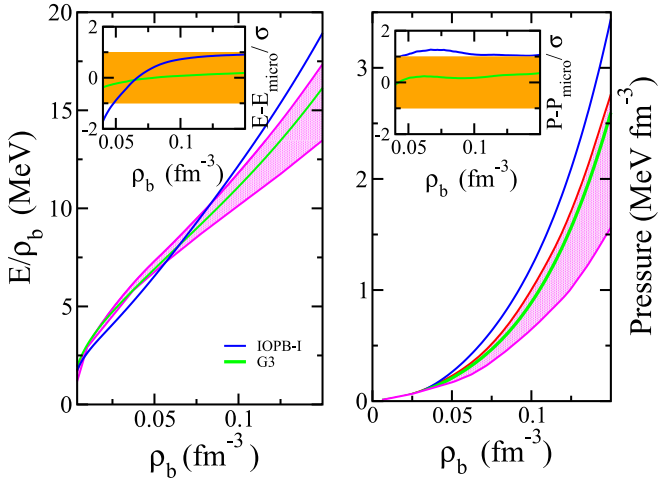

FIG. 1. EoS of nuclear matter below saturation density for pure nuclear matter at $T = 0$ MeV. The shaded magenta region corresponds to the microscopic chiral EFT ($NN + 3N$) [29] calculations. The inner graph represents the difference between the neutron matter energy and pressure and the average energy and pressure with 1σ calculation uncertainty area.

motivate us to use them to study the E-RMF sets with and without the δ meson. δ meson couplings are a necessary feature in the dense asymmetric nuclear matter. In this work we intend to investigate the effects of δ meson in the dilute asymmetric matter in the finite-temperature limit. We also try to explore role of different self and cross couplings at the finite-temperature properties of asymmetric nuclear matter.

B. Finite-temperature properties

The nuclear symmetry energy (NSE) is one of the crucial properties of asymmetric nuclear matter governing several areas of nuclear matter calculations, like reaction dynamics, phase stability, or cooling in the neutron star. Temperature dependence of NSE, on the other hand, provides the much needed knowledge on the dynamical evolution of neutron star and isoscaling analyses of heavy-ion-induced reactions. NSE is not a directly measurable quantity in experiments and is extracted from the observables related to it. Despite numerous theoretical and experimental efforts, it is still not a very precise parameter even for cold nuclear matter. In Fig. 2, we show the variation of free nuclear symmetry energy (FNSE) [more relevant quantity in finite-temperature case, see Eq. (11)] the slope parameter $L_{\rm sym}$, the isovector incompressibility $K_{\rm sym}$, and the isovector skewness $Q_{\rm sym}$ with the density up to two times the saturation density. The free NSE is scaled towards higher magnitude due to decrease in entropy, preserving its characteristic shape at a higher temperature for both IOPB-I and G3 sets. At higher density, the temperature range considered here does not affect FSNE much. The slope parameter, which has a direct correlation with neutron skin thickness, electric-dipole polarizabilities, etc., also follows a similar trend for both the sets. The NSE estimated from these sets are also consistent with the Heavy-ion collision (HIC) Sn + Sn and IAS data [24]. The low values of $F_{\rm sym}$ and $L_{\rm sym}$ are the result of cross couplings of ρ mesons with ω mesons in the IOPB-I set and coupling of σ mesons with ω mesons in the G3 set, which predicts even lower $F_{\rm sym}$ due to the presence of isovector scalar δ mesons. The δ meson has a positive effect on the binding energy and helps to estimate $F_{\rm sym}$, $L_{\rm sym}$, and

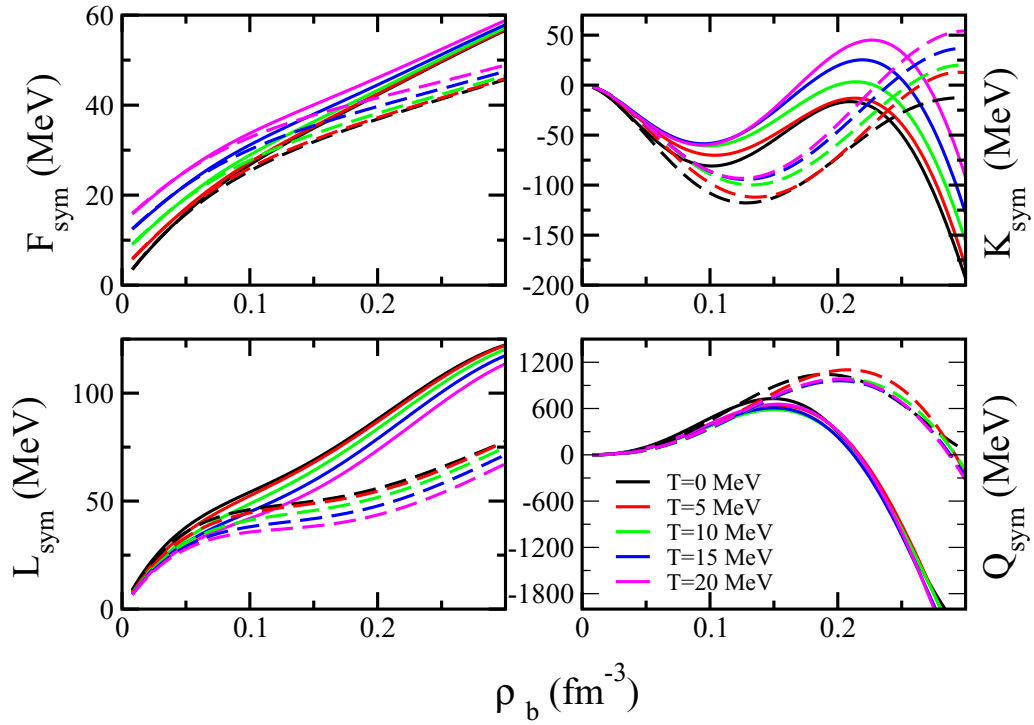

FIG. 2. Free symmetry energy $F_{\rm sym}$, slope parameter L, curvature $K_{\rm sym}$, and isovector skewness parameter $Q_{\rm sym}$ as a function of density at various temperature for IOPB-I (solid lines) and G3 (dashed lines) sets.

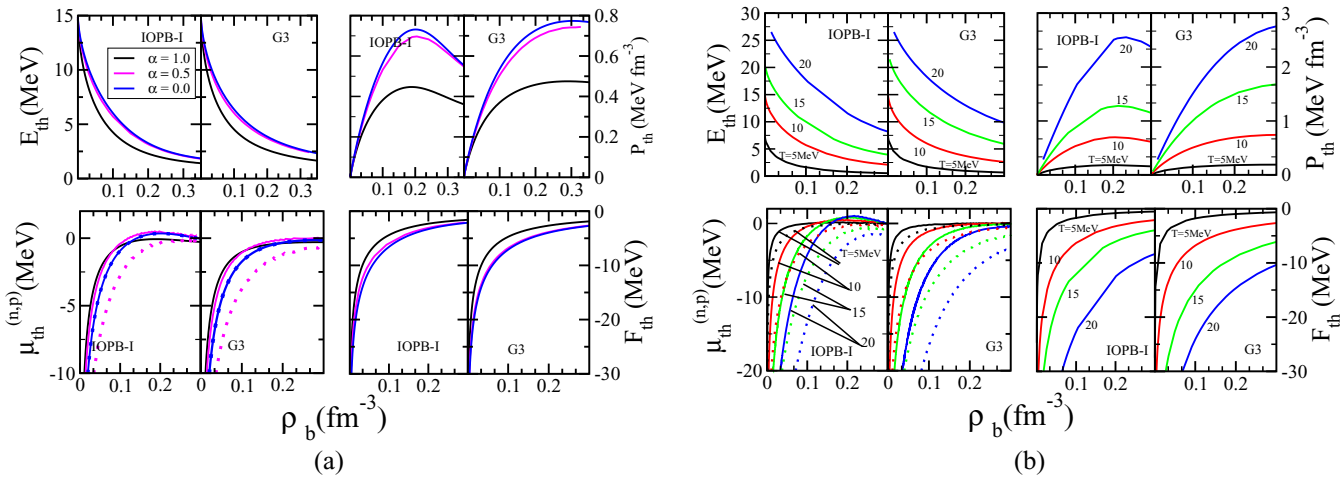

FIG. 3. (a) Thermal energy, pressure, chemical potential, and free-energy density for fixed $T = 10$ MeV for various $\alpha = 0,\ 0.5,\ 1$. (b) Same as in panel (a) but for various $T = 5,\ 10,\ 15,\ 20$ MeV at fixed $\alpha = 0.5$. The solid lines are for neutron chemical potential and the same color dotted line represents the proton chemical potential.

$K_{\rm sym}$ within the permissible limit [22]. The sinusoidal variation of $K_{\rm sym}$ with density is also shown. $K_{\rm sym}$ is constrained recently by combining the data from PSR J0030 + 0451 and GW170817 estimating $K_{\rm sym} = 102^{+71}_{-72}$ MeV within 1σ error [33]. The IOPB-I and G3 both fall within this constraint. The variation of $Q_{\rm sym}$ with density is almost independent of temperature for the IOPB-I set and a small variation is observed for G3 set. The $Q_{\rm sym}$ is the least constrained property in any experiment and several models predict it with a large variation [21].

To study the finite temperature effect, we isolate the thermal part of a given function according to equations (15). The subtraction scheme applies only to those variable which depend on the kinetic-energy density [26]. Figure 3 shows the thermal effect on various state variables at a fixed temperature and α for IOPB-I and the G3 parameter set. The common observation is that (i) at the fixed temperature, the thermal energy decreases with density. The difference due to asymmetry disappears at high densities, thermal effects become weak, and the thermal energy becomes density independent and tends asymptotically to zero. (ii) At very low density, the thermal energy and pressure have a linear T dependence as for a free Boltzmann gas (nondegenerate limit). This linearity is changed when matter becomes increasingly degenerate. (iii) Temperature effects are more prominent in thermal pressure as compared with thermal energy. (iv) The thermal chemical potential becomes saturated after saturation density. In Ref. [25,26], the thermal effects are found to be dominated by the behavior of effective mass. These calculations were done for the Skyrme and APR forces where the effective mass has a different origin when compared with the Dirac mass of relativistic forces [36]. The Dirac mass in the relativistic formalism finds its origin from the spin-orbit potential whereas the effective mass in the nonrelativistic formalism arises from the momentum dependence of the single-particle potential [37]. However, both of these masses impact the thermal contribution to the state variables in a somewhat similar way.

In Fig. 4, the density dependence of the Dirac effective mass for pure neutron matter (PNM) is shown in the left panel. The effective mass for G3 decreases at a relatively slower pace as compared with the IOPB-I set. Due to the presence of the δ meson, the neutron and proton mass gets split, which is not the case for the IOPB-I set due to the absence of the δ meson. In right panel of Fig. 4, the effective mass at the saturation density is plotted for different values of α for the G3 parameter set. This δ-meson mechanism on effective mass is an important phenomenon in studying drip line nuclei of astrophysical interest [38] and is analyzed in experiments such as PREX [39]. The effective mass is the input for the computation of energy, pressure, and chemical potential, which is determined self-consistently. The behavior of effective mass therefore clearly dictates the thermal pressure and thermal energy. The G3 set with larger effective mass estimates a greater thermal contribution on state vari-

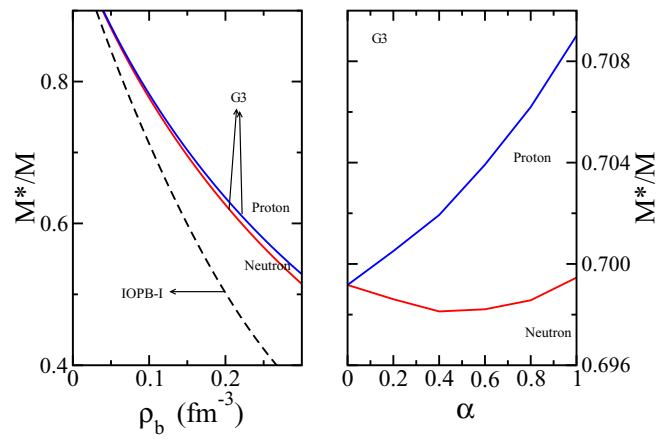

FIG. 4. The effective mass for IOPB-I and G3 set. The left panel shows the mass splitting for PNM in the G3 set (solid lines) as compared with the IOPB-I set (dashed line). The right panel shows the effective mass at saturation density for the G3 set.

ables as compared with the IOPB-I set with smaller effective mass. This is consistent with the Fermi-liquid theory and nonrelativistic calculations [25]. For the IOPB-I set, the thermal pressure increases and then decreases beyond the saturation density but for G3 it saturates at higher density. Furthermore, the quantitative difference in thermal energy and pressure between IOPB-I and G3 set is due to the difference in the self-coupling of isoscalar-scalar σ meson which is responsible for the $3N$ interaction, which plays an important role in determining the thermal pressure and energy. This behavior is analogous to chiral $2N$ and $3N$ interactions, although with a larger thermal contribution as compared with the many-body self-consistent Green's function method [40]. The decrease in thermal pressure after reaching its maximum is the combined effect of incompressibility of the EoS at zero temperature and the rapidity of the finite-temperature pressure. Knowledge of the thermal effect on the relevant state variable is important in large-scale simulations such as supernovae, neutron-star crust, and neutron-star binary simulations, where the EoS at any given temperature can be estimated by adding the thermal contribution. This will reduce the computation cost for these simulations as one do not have to carry out the full self-consistent calculations at every temperature [41,42].

The chemical potential at fixed $T = 10$ MeV has interesting behavior. μ_n at $\alpha = 1$ is crossed over by μ_n at $\alpha < 1$ with increasing density while that is not the case for μ_p. Moreover, the crossings of μ_n occur at a higher density at larger temperature. Chemical potential becomes saturated at higher density because of the increasing degeneracy at higher density. The different nature of chemical potential is again the consequence of effective mass along with the self and cross-coupling of the σ meson. The thermal free energy tends to zero with increasing density, like the chemical potential. Comparing the IOPB-I and G3 sets for thermal properties shows that the parameter set G3 has additional δ-meson coupling whose contribution increases with density. This contribution directly impacts the effective mass [see Eq. (6a)], which in turn decides the behavior of various variables studied above. The δ meson along with the σ meson therefore makes direct contributions to the thermal properties of the EoS.

Figure 5 shows the variation of the thermal index Γ with density for the IOPB-I and G3 sets at fixed temperature and asymmetry. By comparing the case of fixed temperature and α with those of thermal energy and pressure (Fig. 3), it is certain that Γ depends mainly on (i) the stiffness of pressure, (ii) the behavior of effective mass with respect to density, and (iii) α. For $\rho \to 0$, Γ approaches the nonrelativistic ideal-gas index $\frac{5}{3}$. Γ is very sensitive to the asymmetry at a fixed temperature, which is opposite to the nonrelativistic calculations where the peak of Γ is insensitive to asymmetry [26]. Furthermore, it is immune to temperature change for fixed α. For the IOPB-I set the maximum Γ is 2.1 for PNM and 1.97 for symmetric nuclear matter (SNM). The G3 set reports these values to be 1.96 and 1.87, respectively. The G3 set with larger effective mass estimates the lower pressure and therefore a larger thermal index as compared with the IOPB-I set with lower effective mass. These results of Γ from the newly developed E-RMF sets are consistent with the dynamics of the neutron-star merger where Γ is taken as 1.5 and 2, indicating that these two sets can be used for the calculations of such events [43]. However, in the astrophysical simulation like a binary star and a proto-neutron star, Γ is taken as a constant, whereas here it varies with density. The behavior of Γ is in agreement as with EFT theory [40].

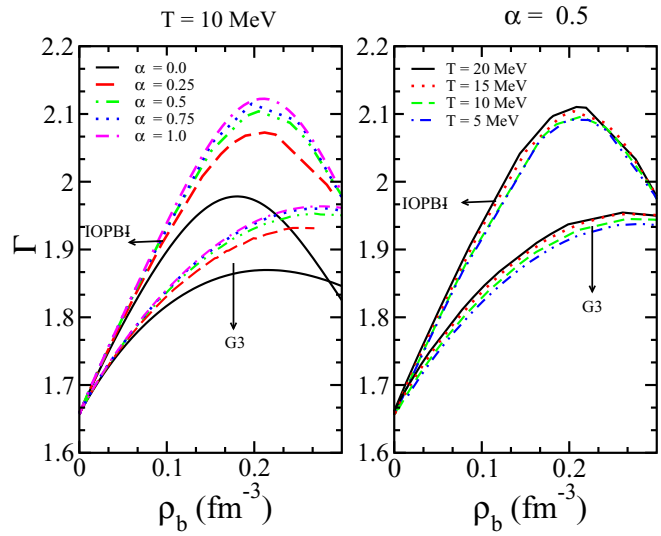

FIG. 5. Thermal index for IOPB-I (solid lines) and G3 sets (dash line) for fixed temperature in the left panel and fixed $\alpha = 0.5$ in the right panel.

Nuclear matter incompressibility along the isothermal (K^T) and isentropic (K^S) paths is shown in Fig. 6 for IOPB-I and G3 sets for two values of α (i.e., 0.3 and 0.5). These values are taken due to their relevance in a core-collapse supernova. The incompressibility at saturation in cold nuclear matter is governed by self-coupling of the σ meson. The incompressibility of both the IOPB-I and G3 sets falls within the accepted empirical value, as prescribed by the giant monopole resonance, i.e., 240 ± 20 MeV. At finite temperature, we define incompressibility within two channels: one being the isothermal incompressibility and the other the isentropic incompressibility defined according to Eqs. (23) and (24), respectively. The isentropic incompressibility is the more relevant quantity in the context of a supernova explosion because the timescale of collapse is less than one second and the process is adiabatic instead of isothermal. It prompts us to use energy instead of free energy [see Eq. (24)]. The incompressibility (both isothermal and isentropic) decreases quadratically with temperature with G3 having a higher magnitude at each temperature and entropy. It also decreases with increasing asymmetry. We show the temperature dependence of $K^{T,S}/K^0$ and $(\rho^{T,S}/\rho^0)^2$ in the context of their relation with respective incompressibility [see Eqs. (23) and (24)]. Their behavior remains almost similar, irrespective of any change in asymmetry. These results satisfy the calculations carried out using microscopic approaches [44,45], thereby suggesting that these newly developed parameters not only can describe finite nuclei and cold nuclear matter but also can be used to study the phenomenon at finite temperature such as proto-neutron star and supernova explosions.

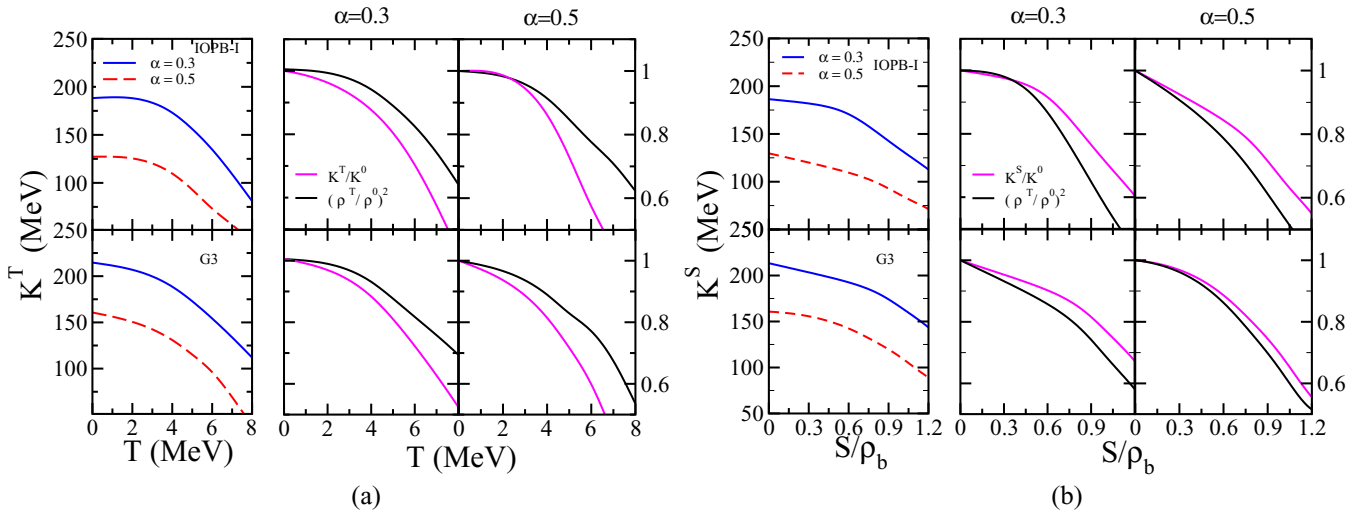

FIG. 6. (a) Isothermal and (b) isentropic incompressibility at $\alpha = 0.3$ and 0.5 for IOPB-I and G3 sets at saturation density.

C. Liquid-gas phase transition

The asymmetric nuclear matter is a two-component system with two conserved charges Q (B, I_3). In a two-component system, although the total charge remains conserved, the ratio can be different in different phases. The constraint on T, Q, and ρ, which determine the energetic of the system, forces vapor pressure and chemical potential to change during the phase transition. Apart from mechanical instability, the diffusive instability (fluctuations on the charge concentration) appears and is more relevant to describe the asymmetric matter. The phase transition in the asymmetric matter is therefore described by the following three regions:

(1) Isothermal spinodal (ITS): describe the mechanical instability given by $\frac{\partial P}{\partial \rho_b}$. It defines the critical temperature in symmetric matter.
(2) Diffusive spinodal (DS): describe the chemical instability. It essentially means that energy is required to add extra protons to the system at a fixed temperature and pressure. The critical isobar P_c is estimated by finding a inflation point $\frac{\partial \mu_p}{\partial \alpha}|_{P_c} = 0$. The corresponding $T = T_c$ and $\rho = \rho_c$ are called the critical temperature and density, respectively.
(3) Coexistence curve (CE): Set of points where Eq. (20) along with the Gibbs conditions are satisfied. This curve may contain the critical points. Unlike the symmetric-matter case, here the CE is binodal or two dimensional.

The complexity of the phase transition in the asymmetric nuclear matter is shown in Fig. 7. As one moves from symmetric to asymmetric matter, a new behavior distinct to the two-component system is allowed. Asymmetry is held constant during the phase transition, which forces the system to change its chemical potential and consequently the pressure (shown by the dashed line in the left panel of Fig. 7). Due to charge fluctuation during this phase transition, the diffusive instability appears and plays more important role than mechanical instability in describing the phase transformation. The right panel of Fig. 7 shows all three curves, i.e., ITS, DS, and CE, and it is visible that diffusive instability has a larger area as compared with mechanical instability.

Binodal as per the Gibbs condition given in Eq. (21) at $T = 10$ MeV is plotted in Fig. 8 by geometrical construction where a rectangle is drawn on the chemical-potential isobars of neutrons and protons [46]. It is characterized by the point of equal construction (EC). The point of maximal asymmetry (MA) and the critical point which determine the edge of the instability area. In the phase coexistence region, the proton fraction of two-phase changes (a unique feature of two-component systems) and the phase with higher asymmetry exhibits a lower density or vice versa. At the critical temperature of symmetric matter, all the three points (EC, MA, CP) coincide and the surface becomes a point. The vertical dashed magenta line indicates that, during the phase transition, α remains constant and both phases follow different paths, i.e., liquid follows the path A1-A2 while the gas phase evolves from B1 to B2 during the isothermal compression.

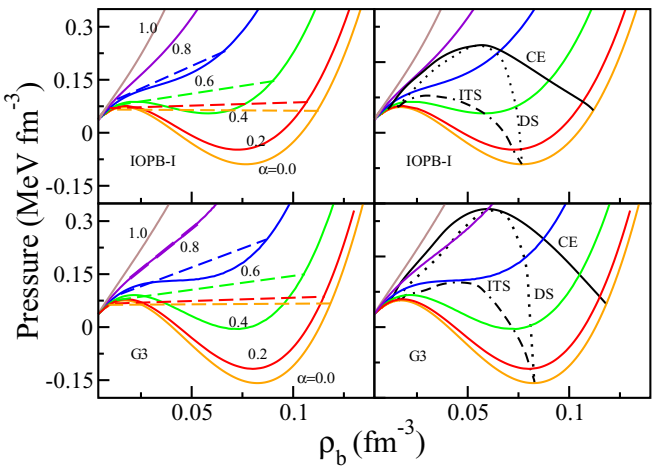

FIG. 7. EoS of nuclear matter at various α at $T = 10$ MeV along with the ITS, DS, and CE curves for the IOPB-I and G3 sets.

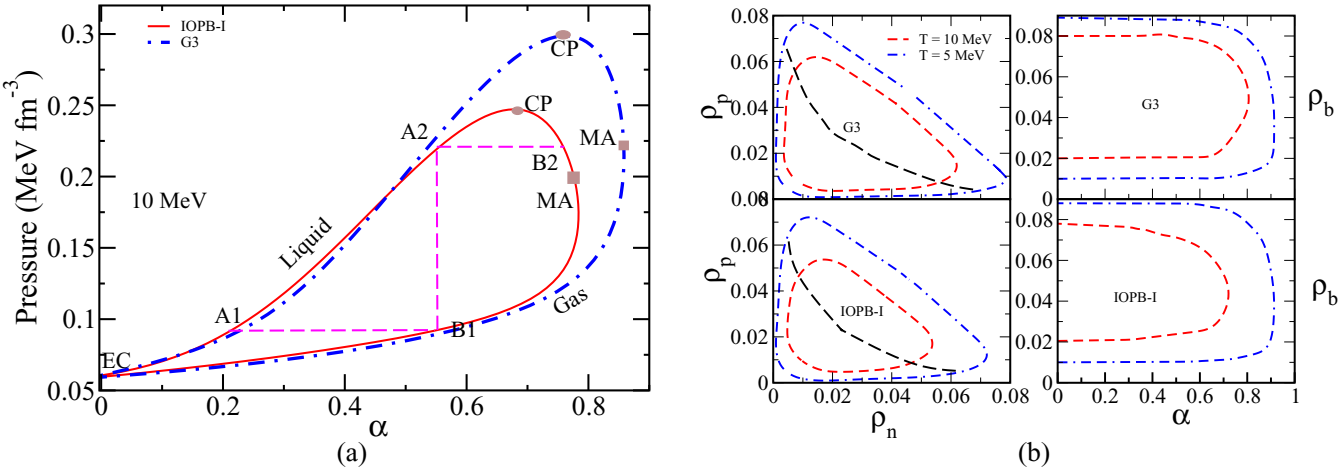

FIG. 8. (a) The binodal surface on the P-α plane is shown on the left and (b) the spinodal boundary in the ρ_n-ρ_p plane and the α-ρ_b plane is shown on the right. The black dashed line on the spinodal shows the critical points.

Finally, the system leaves the instability at A2. This condition is called stable condensation. On the other hand, when the system is prepared with $\alpha > \alpha_c$ (α at CP), it operates in the gaseous phase only, and this unique phenomenon is called retrograde condensation. The spinodal according to Eq. (20) is plotted on the right side of Fig. 8 on both the ρ_n-ρ_p and α-ρ_b planes. Figures 7 and 8 provide a complete description of the phase transition in asymmetric nuclear matter.

In symmetric nuclear matter, the compressibility is the deciding factor for critical parameters of phase transition whereas, the phase transition in the asymmetric matter is characterized by symmetry energy. This can be verified from Eq. (12) where the contribution of iso-spin asymmetry is reflected from the free symmetry energy $F_{\rm sym}$ and its slope $L_{\rm sym}$. $K_{\rm sym}$ and $Q_{\rm sym}$ are the higher-order derivative of FNSE in the Taylor series which are still not well constrained. We have used two E-RMF sets IOPB-I and G3 to account for the various EoS properties on the phase transition in the asymmetric matter. The detailed analysis of the phase transition in symmetric matter using the IOPB-I and G3 sets is discussed in Ref. [19]. For ANM, the asymmetry in density is introduced by the ρ meson and is dictated by cross coupling $\lambda_\omega(R^2W^2)$. The G3 and IOPB-I set has $\lambda_\omega = 0.038$ and 0.024, respectively. The corresponding values of J and L at $T = 0$ MeV are given in Table I, whereas their finite temperature dependence is shown in Fig. 2. The G3 set has an additional mass asymmetry introduced by the δ meson. The δ meson allows one to vary $L_{\rm sym}$ without altering the symmetry energy $F_{\rm sym}$. At a given temperature, the G3 set has a larger coexistence area and large values of CP and MA as compared with the IOPB-I set due to the δ meson. A large coexistence area favors highly asymmetric gas in coexistence with less asymmetric dense fluid. This has a direct consequence for the core-crust transition and the crust structure of neutron stars. Opposite to SNM, where ζ_0 plays the determining role, the value of λ_ω decides the ANM which in turn affects $L_{\rm sym}$. A greater λ_ω usually gives smaller $L_{\rm sym}$ and vice versa.

The spinodal for the G3 set also has a larger area at any given temperature as compared with the IOPB-I set. One can observe the major variation among two sets in the coexistence densities in the α-ρ_b plane. This means that the densities where different structure in the nonhomogeneous phase occur will be different. This property is again determined by $L_{\rm sym}$. The G3 set with smaller $L_{\rm sym}$ estimates a larger α and ρ_c at any given temperature. This is shown in Fig. 9, where the dependence of α and ρ_c is shown on temperature. The α-T plots signify the temperature at which the diffusive instability disappears (also called the critical temperature). This critical temperature is not similar to symmetric matter where mechanical instability decides the phase transition but is determined according to $\frac{\partial \mu_p}{\partial \alpha}|_{P,T} = 0$ and $\frac{\partial^2 \mu_p}{\partial \alpha^2}|_{P,T} = 0$. In the E-RMF sets with constant couplings, the inflation point for the proton and neutron coincides, having synchronous behavior. This might not be the case with density-dependent coupling sets [47,48]. α decreases smoothly at low temperatures but, after $T > 0.5T|_{\alpha=0}$, there is a steep fall in α. The G3 set estimates larger α at a particular T due to its smaller value of $L_{\rm sym}$ and greater value of λ_ω. This same trend is observed in ρ_c. These trends are similar to Refs. [6,16], where any one coupling in a parameter set were varied keeping other fixed to obtain different $L_{\rm sym}$. The agreement of those trends

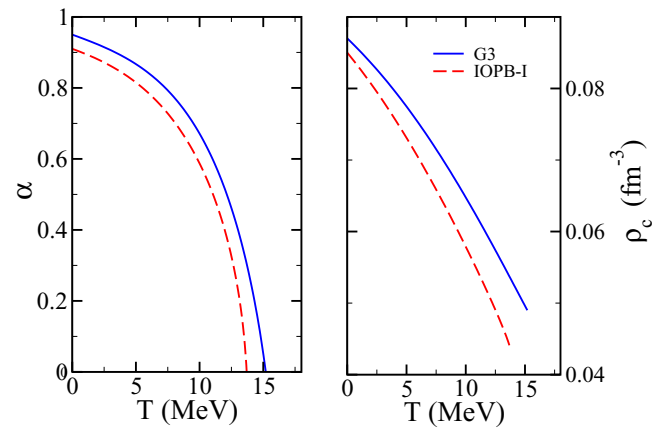

FIG. 9. α as a function of temperature and corresponding ρ_c for the IOPB-I and G3 sets.

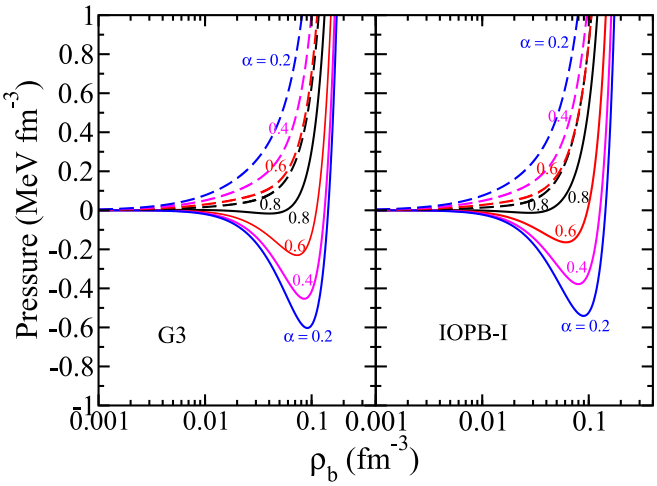

FIG. 10. The EoS with and without electrons. The solid line represents the nuclear matter without electrons and the dashed line represents the same with electrons.

while comparing two different parameter sets with almost the same symmetry energy indicates that the correlation between different properties of the phase transition still holds, as in the case of SNM [49], and these can be exploited to constraint the EoS, which does not take critical temperature into the account [19,50].

D. Effect of electrons

In a physical system, the electrons are present so that the Coulomb energy does not diverge. They are included in the EoS as a free noninteracting relativistic Fermi gas described by [17]

$$L_e = \bar{\psi}_e[i\gamma_\mu \partial^\mu - m_e]\psi_e, \tag{25}$$

where L_e is the Lagrangian, and m_e is the mass of the electron. Since the electrons only compensate the proton charge, we have $\rho_p = \rho_e = \frac{1}{\pi^2}\int k^2 dk(n_{ke} - \bar{n}_{ke})$. Where n_{ke} and $\bar{n}_{ke}$ are the Fermi integral for electrons and positrons. Figure 10 shows the effect of electrons on the EoS for the IOPB-I and G3 parameter sets at $T = 0$ MeV. The effect of electrons is dominant for matter with less asymmetry because the electron density becomes high to compensate for the larger proton density. Electrons are taken as noninteracting particles and therefore the underlying nature of a parameter set in unaltered. Electrons have high Fermi energy and, therefore, make the system devoid of the instability. Both the IOPB-I and G3 sets have no spinodal when electrons are included for $T = 5$ MeV. No spinodal means that stellar matter at β equilibrium will be uniform at temperature above 5 MeV [12]. This is consistent with the various calculations of neutron star core crust transition.

To further understand the implication of electrons in the EoS, we study the adiabatic index. In processes such as supernovae explosions and neutron stars, the compression and rarefaction modes of vibration are adiabatic or isentropic instead of isothermal [26]. The adiabatic index is related to the stiffness of EoS and is given by

$$\Gamma_s = \frac{\rho_b}{P}\frac{\partial P}{\partial \rho_b}\Big|_s. \tag{26}$$

$\Gamma_{s=0}$ for the two models employed here is shown in Fig. 11. The solid black curve represents the nucleon only while the red dashed curve includes the contribution from electrons. $\Gamma_{s=0}$ corresponding to nucleons goes negative in some density regions showing the mechanical instability. For low and high densities it varies asymptotically. The inclusion of electrons restore the mechanical instability and the value of $\Gamma_{s=0}$ increases gradually around subsaturation density and becomes asymptotically constant at low and high densities. These observations can be understood quantitatively by examining the baryon and electron pressure as shown in Fig. 10. For $\rho \to 0$, $\Gamma_{s=0}$ tends to $\frac{4}{3}$ which is due to the relativistic electrons and is an important requirement for the stability of supernova simulation. As asymmetry rises, this value goes to $\frac{5}{3}$ for pure neutron matter. Although the underlying properties for Γ_s are the same for both models, except for the position of instability and the highest value of Γ_s in the case of matter with electrons, they are essentially determined by the pressure due to baryons. The parameter sets IOPB-I and G3 do not break the causality condition on speed of sound [51]. The presence of electrons in the system also impacts the speed of sound $C_s^2 = \frac{\partial p}{\partial E}$. Addition of electrons do not yield the nonphysical region in low density as is seen in the nuclear matter system without leptons. At higher density, the electrons impart significant impacts on the more symmetric matter, making it smoother as compared with the asymmetric matter.

IV. SUMMARY AND OUTLOOK

The primary aim of this work was to study the thermal properties of hot and dilute isospin asymmetric nuclear matter within the effective relativistic mean-field (E-RMF) formalism. Although the thermodynamics of symmetric nuclear matter is explored, the isospin effects are still not understood at finite temperature. In this study, we consider the dilute homogeneous nuclear matter at different values of temperature and isospin asymmetry because of their relevance in astrophysical simulations. We study the temperature dependence of free nuclear symmetry energy $F_{\rm sym}$ and its higher-order derivatives. $F_{\rm sym}$ increases with temperature at a given density due to a decrease in entropy density. The higher-order derivative of $F_{\rm sym}$ preserves the zero temperature behavior with a slight change in magnitude, which shows that one can use the zero-temperature value of these parameters to compare the relevant quantities at any given temperature.

To study the finite-temperature effect, we separate the thermal component from the zero-temperature EoS. It is observed that the thermal effects in the E-RMF formalism depend mainly on the density dependence of Dirac effective mass. The Dirac effective mass is calculated self-consistently, which depends on the σ and δ mesons. A larger Dirac effective mass corresponds to larger thermal effects on the state variables. A similar effect of effective mass on the thermal contribution is seen in nonrelativistic formalisms, although both the Dirac mass and effective mass in nonrelativistic

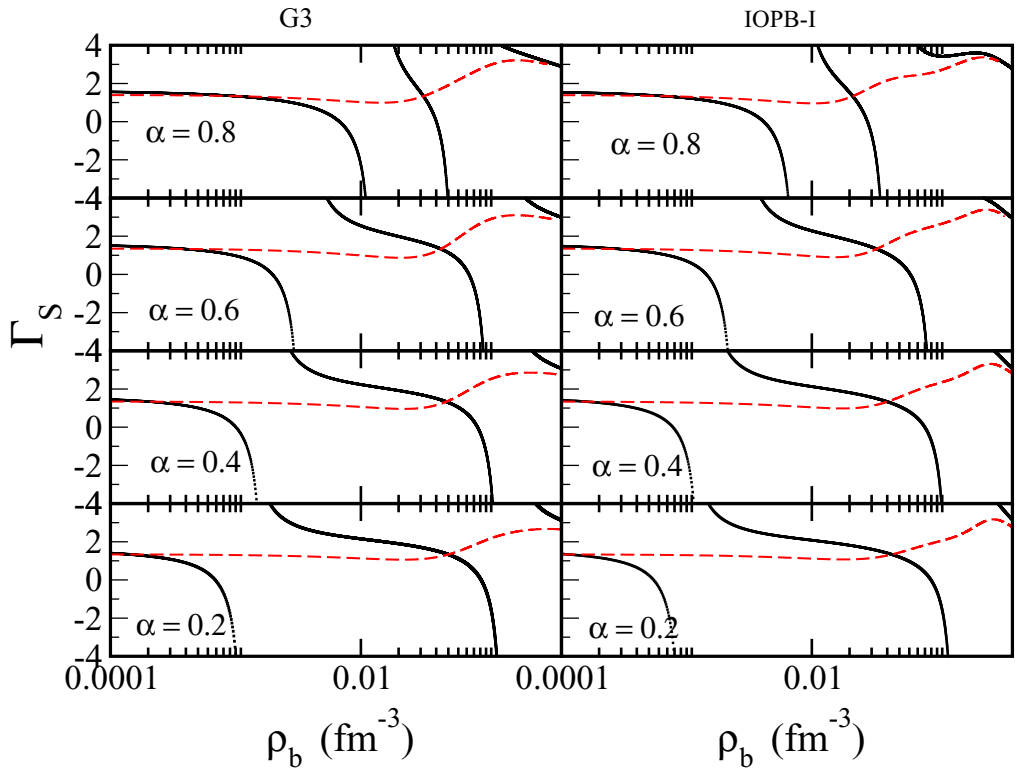

FIG. 11. Adiabatic index $\Gamma_{s=0}$ for the G3 and IOPB-I sets with various asymmetry. The solid black line includes only nucleons while the red line indicates the presence of electrons.

conditions defer in their origin. The thermal effects are also sensitive to isospin asymmetry. The isospin asymmetry also impacts the peak of the isothermal thermal index Γ at a fixed temperature. The isothermal (K^T) and isentropic (K^S) incompressibility varies parabolically with temperature, implying a nonlinear effect of temperature on the EoS. The trends of incompressibilities are in agreement with available microscopic calculations.

The model dependence of these calculations is discussed by using two E-RMF sets, i.e., IOPB-I and G3, because they estimate the nuclear matter observables within the various constraints imposed by various theoretical and experimental analyses. They provide us with the opportunity to study the effect of various meson couplings because these models have comparable symmetry energy at saturation but differ in the value of slope parameter $L_{\rm sym}$, which is an important parameter in deciding the instability of a system. It is observed that the underlying nature of the thermal contribution to a state variable at a given isospin asymmetry remains the same with increasing temperature across the forces used in this study. The change in magnitude of the thermal contribution is principally attributed to their zero-temperature variation, which is the result of their different nuclear matter observables such as incompressibility, symmetry energy, and its higher-order derivatives.

The presence of the δ meson in the G3 set and its absence in the IOPB-I set prompts us to study the behavioral change in the liquid-gas phase transition. The phase transition is studied for the asymmetric nuclear matter considering a two-component system with two conserved charges, i.e., Baryon number and isospin. The G3 set, due to its low $L_{\rm sym}$, estimates the higher value of the maximal asymmetry and critical pressure. The presence of the δ meson has a positive effect on binding energy and therefore influences the boundary of the spinodal. The critical density and asymmetry are also larger for the G3 set, which can be attributed to its lower $L_{\rm sym}$. The value of $L_{\rm sym}$ is determined mainly by cross coupling of ρ and ω mesons with the δ meson. One can say that a larger value of λ_ω estimates the larger instability in asymmetric nuclear matter. Critical asymmetry is a quadratic function of temperature and exhibits different behavior in the low- and high-temperature range. These trends are also consistent with other relativistic studies available in the literature.

Finally, we study the effect of electrons in the EoS of nuclear matter and its instability. Electrons due to their high Fermi energy make the system devoid of instabilities. We study the adiabatic index ($\Gamma_{S=0}$) of matter with and without the inclusion of electrons. The Γ_S with electrons becomes asymptotically constant at low and high densities, with a small variation near the saturation density. The density of this hump predominantly depends on the baryon pressure. The electron being a noninteracting particle does not alter the underlying nature of the force parameter.

The present calculations can be extended to study the various astrophysical processes such as the supernova explosion and neutron-star crust, where the nuclear matter is dilute and at some finite temperature. The low-density matter results in the formation of clusters, which subsequently impacts various cooling and transportation processes. Furthermore, the idea of

a thermal effect on state variables will help to reduce the computational cost and time of the numerical calculations in large simulations such as impersonating supernovae explosions and neutron-star binary collisions. Such an analysis is important to estimate an equation of state for a wide range of density and will be carried out in future work.

[1] S. M. Couch, Philos. Trans. R. Soc., A **375**, 20160271 (2017).
[2] V. Roma, J. Powell, I. S. Heng, and R. Frey, Phys. Rev. D **99**, 063018 (2019).
[3] B. Müller, H.-T. Janka, and H. Dimmelmeier, Astrophys. J., Suppl. Ser. **189**, 104 (2010).
[4] C. J. Stapleford, C. Fröhlich, and J. P. Kneller, Phys. Rev. D **102**, 081301(R) (2020).
[5] R. Sawada and K. Maeda, Astrophys. J. Lett. **886**, 47 (2019).
[6] N. Alam, H. Pais, C. Providência, and B. K. Agrawal, Phys. Rev. C **95**, 055808 (2017).
[7] S. Nishizaki, T. Takatsuka, and J. Hiura, Prog. Theor. Phys. **92**, 93 (1994).
[8] M.-Q. Liu, Res. Astron. Astrophys. **11**, 91 (2010).
[9] E. F. Brown, A. Cumming, F. J. Fattoyev, C. J. Horowitz, D. Page, and S. Reddy, Phys. Rev. Lett. **120**, 182701 (2018).
[10] B. P. Abbott *et al.* (LIGO Scientific Collaboration and Virgo Collaboration), Phys. Rev. Lett. **119**, 161101 (2017).
[11] B. P. Abbott *et al.*, Astrophys. J. Lett. **848**, L12 (2017).
[12] S. S. Avancini, D. P. Menezes, M. D. Alloy, J. R. Marinelli, M. M. W. Moraes, and C. Providência, Phys. Rev. C **78**, 015802 (2008).
[13] G. Grams, A. M. Santos, P. K. Panda, C. Providência, and D. P. Menezes, Phys. Rev. C **95**, 055807 (2017).
[14] B. Kumar, S. K. Patra, and B. K. Agrawal, Phys. Rev. C **97**, 045806 (2018).
[15] B. Kumar, S. K. Singh, B. K. Agrawal, and S. K. Patra, Nucl. Phys. A **966**, 197 (2017).
[16] B. Sharma, S. Sathees, M. Meghaa, and T. Jha, Nucl. Phys. A **1002**, 121974 (2020).
[17] S. S. Avancini, L. Brito, P. Chomaz, D. P. Menezes, and C. Providência, Phys. Rev. C **74**, 024317 (2006).
[18] S. S. Avancini, L. Brito, D. P. Menezes, and C. Providência, Phys. Rev. C **70**, 015203 (2004).
[19] V. Parmar, M. K. Sharma, and S. K. Patra, J. Phys. G **48**, 025108 (2021).
[20] M. Del Estal, M. Centelles, X. Viñas, and S. K. Patra, Phys. Rev. C **63**, 024314 (2001).
[21] A. Kumar, H. Das, S. Biswal, B. Kumar, and S. Patra, Eur. Phys. J. C **80**, 1 (2020).
[22] S. K. Singh, S. K. Biswal, M. Bhuyan, and S. K. Patra, Phys. Rev. C **89**, 044001 (2014).
[23] I. Bednarek, J. Sładkowski, and J. Syska, Symmetry **12**, 898 (2020).
[24] M. B. Tsang, Y. Zhang, P. Danielewicz, M. Famiano, Z. Li, W. G. Lynch, and A. W. Steiner, Phys. Rev. Lett. **102**, 122701 (2009).
[25] C. Constantinou, B. Muccioli, M. Prakash, and J. M. Lattimer, Phys. Rev. C **89**, 065802 (2014).
[26] C. Constantinou, B. Muccioli, M. Prakash, and J. M. Lattimer, Phys. Rev. C **92**, 025801 (2015).
[27] H. Müller and B. D. Serot, Phys. Rev. C **52**, 2072 (1995).
[28] S. Haddad, Int. J. Mod. Phys. E **12**, 125 (2003).
[29] K. Hebeler, J. M. Lattimer, C. J. Pethick, and A. Schwenk, Astrophys. J. **773**, 11 (2013).
[30] H. A. Bethe, Annu. Rev. Nucl. Sci. **21**, 93 (1971).
[31] T. Marketin, D. Vretenar, and P. Ring, Phys. Rev. C **75**, 024304 (2007).
[32] P. Danielewicz and J. Lee, Nucl. Phys. A **922**, 1 (2014).
[33] J. Zimmerman, Z. Carson, K. Schumacher, A. W. Steiner, and K. Yagi, arXiv:2002.03210.
[34] B.-J. Cai and L.-W. Chen, Nucl. Sci. Tech. **28**, 185 (2017).
[35] U. Garg and G. Colò, Prog. Part. Nucl. Phys. **101**, 55 (2018).
[36] M. Jaminon and C. Mahaux, Phys. Rev. C **40**, 354 (1989).
[37] L.-W. Chen, C. M. Ko, and B.-A. Li, Phys. Rev. C **76**, 054316 (2007).
[38] C. J. Horowitz and J. Piekarewicz, Phys. Rev. Lett. **86**, 5647 (2001).
[39] S. Abrahamyan *et al.* (PREX Collaboration), Phys. Rev. Lett. **108**, 112502 (2012).
[40] A. Carbone and A. Schwenk, Phys. Rev. C **100**, 025805 (2019).
[41] H. Shen, H. Toki, K. Oyamatsu, and K. Sumiyoshi, Prog. Theor. Phys. **100**, 1013 (1998).
[42] C. A. Raithel, F. Özel, and D. Psaltis, Astrophys. J. Lett. **875**, 12 (2019).
[43] H. Yasin, S. Schäfer, A. Arcones, and A. Schwenk, Phys. Rev. Lett. **124**, 092701 (2020).
[44] M. Modarres and G. H. Bordbar, Phys. Rev. C **58**, 2781 (1998).
[45] I. Bombaci, T. Kuo, and U. Lombardo, Phys. Lett. B **311**, 9 (1993).
[46] J. M. Lattimer and D. Ravenhall, Astrophys. J. **223**, 314 (1978).
[47] A. Fedoseew and H. Lenske, Phys. Rev. C **91**, 034307 (2015).
[48] T. Nikšić, D. Vretenar, P. Finelli, and P. Ring, Phys. Rev. C **66**, 024306 (2002).
[49] O. Lourenço, M. Dutra, and D. P. Menezes, Phys. Rev. C **95**, 065212 (2017).
[50] S. Yang, B. N. Zhang, and B. Y. Sun, Phys. Rev. C **100**, 054314 (2019).
[51] H. C. Das, A. Kumar, B. Kumar, S. K. Biswal, T. Nakatsukasa, A. Li, and S. K. Patra, Mon. Not. R. Astron. Soc. **495**, 4893 (2020).